Int. J. Heat Mass Transfer. Vol. 35, No. 10, pp. 2403–2411, 1992
Printed in Great Britain

0017-9310/92 $5.00 + 0.00
Pergamon Press Ltd

Evaporation of non-dilute and dilute monodisperse droplet clouds

SHWIN-CHUNG WONG and JYH-CHENG CHANG

Department of Power Mechanical Engineering, National Tsing Hua University, Hsinchu, Taiwan 30043, Republic of China

(*Received* 20 *May* 1991 *and in final form* 24 *October* 1991)

Abstract—The evaporation of droplets in non-dilute and dilute monodisperse droplet clouds has been studied both experimentally and theoretically. This study presents quantitative experimental data for monodisperse cloud evaporation. Experiments are performed in an insulated evaporation tube under weakly convective flow conditions at atmospheric pressure. Nearly monosize tetralin clouds having a mean diameter of 30 μm are used for the experiment. For a non-dilute cloud investigated, the evaporation rate is significantly lower than that of a single droplet and evaporation may stop due to saturation. An improved version of droplet-in-bubble model, adopted to describe the evaporation within non-dilute monodisperse clouds, exhibits excellent simulation of the experiments.

1. INTRODUCTION

STUDIES on spray evaporation find applications in a variety of practical situations, such as spray drying, insecticide sprays, fire extinction by water sprays, and combustion in power systems using fuel spray injection. In most engineering applications the liquid is atomized into sprays to mix with the ambient gases. Near the atomizer, the droplets might not fully form and liquid sheets and ligaments might still exist. Shortly downstream droplets are formed but they have not been dispersed. In this dense spray region, the typical distance between droplets is approximately one order of magnitude larger than the average droplet diameter. Further downstream the spray will be well dispersed and the droplet distance becomes much larger than the average droplet diameter. This region is called the dilute spray region. While the spray behavior in the dilute spray region has been well treated [1], the behavior in the non-dilute spray region requires further investigation. For example, turbulence dispersion, drop interaction and limitation on the evaporation rate, collision and coalescence, and polydispersity of the spray, all exist and require further investigation. The present work deals with dense droplet clouds with the focus on the effects of droplet interaction on evaporation.

Non-dilute sprays exhibit very different behavior from dilute sprays due to collective interaction among the closely spaced vaporizing droplets. An example is the group evaporation and combustion phenomena in the burning of sprays. Both experimental observations [2] and theoretical calculations [3] have indicated that individual droplet combustion is not favored in the fuel-rich region of the spray core. The need to study droplet interaction on evaporation within non-dilute sprays has long been acknowledged for practical situations [4]. To examine the effects of droplet interaction on evaporation and combustion, a large number of investigations have been performed. Experiments have been conducted for the combustion of multi-droplet arrays [5, 6] and single streams of interacting droplets [7, 8]. Theoretical calculations also have been performed for multi-droplet systems [9, 10]. All these studies indicated that evaporation or burning rates decreased monotonically with decreasing droplet spacing. Single-droplet theories of evaporation and combustion are, therefore, inapplicable to non-dilute sprays. In spite of the recognition of droplet interaction on evaporation, quantitative experiments revealing the fundamentals of evaporation in non-dilute sprays have been unavailable, largely due to experimental difficulties.

A variety of theories, on the contrary, have been proposed to simulate the evaporation process in non-dilute sprays or clouds. A first approach, applicable to quiescent monodisperse clouds, simplified the cloud as a periodically structured lattice of an infinite extension and the evaporation of each droplet could be considered as a droplet vaporizing quasi-steadily in a 'bubble' [11–13]. This concept arose from Zung [11], who assumed the bubble to be an isothermal and isobaric closed sphere. Assuming a solely diffusive transport mechanism, the concentration profile in the bubble was determined with a volume-averaged concentration imposed at the bubble boundary. The volume of the sphere was the space equally shared by each droplet. Tishkoff [12] improved Zung's crude consideration in the bubble region by solving the coupled conservation equations of energy and species with a non-unity Lewis number. Bellan and Cuffel [13] improved Tishkoff's treatment of boundary conditions by arranging the space among the droplets into two different regions: the spheres of influence (bubbles) associated with each droplet and the edge region between the bubbles. The radius of the bubbles

NOMENCLATURE

C_p	gas phase heat capacity [cal g^{-1} °C^{-1}]	V_e	volume of edge region for each droplet, $\{1-N\cdot[(4/3)\cdot\pi\cdot r_s^3]\}/N$ [cm^3]
d	droplet diameter [μm]	Y	mass fraction.
$\bar{d}$	mean droplet diameter [μm]		
D	mass diffusivity [cm^2 s^{-1}]	Greek symbols	
k	thermal conductivity [cal °C^{-1} cm^{-1} s^{-1}]	α	thermal diffusivity [cm^2 s^{-1}]
L	latent heat [cal g^{-1}]	μ	viscosity [g cm^{-1} s^{-1}]
N	number density [cm^{-3}]	ρ	density [g cm^{-3}].
r	radial coordinate [cm]		
Re	Reynolds number, $\rho[(v_d-v_g)]\cdot d/\mu$		
s	droplet separation distance [μm]	Subscript	
t	time [s]	e	edge region
T	temperature [°C]	s	droplet surface
v_d	droplet velocity [cm s^{-1}]	0	initial
v_g	gas velocity [cm s^{-1}]	∞	ambient.

was the half-distance between the centers of two neighboring droplets. The spray was considered as closely packed face-centered cubic droplet lattice. Global conservation equations of species and energy along with an averaged equation of state were used to describe the evaporation process. In the formulation, the bubble region was time-dependent and spatially distributed but the edge region was lumped. The Lewis number was, however, assumed to be unity. Bellan and Cuffel [13] compared their results with those of the dilute spray evaporation theory of Law [14] (Law's theory treated the vapor accumulation effect simply by dynamically adjusting the far-field vapor concentration and temperature of single droplets). Considerable overestimation of evaporation rates was found in Law's results. Recently, Jang and Chiu [15] attempted to deal with the transient evaporation process associated with a droplet in a non-dilute spray suddenly injected into a high-temperature environment. To account for the interaction from neighboring droplets, they replaced previous treatments at the bubble boundary and edge with an imposed pair-distribution function, which represents the joint probability of finding another droplet at a certain distance. All these models predicted strong droplet interaction in non-dilute sprays.

As far as convective evaporation within non-dilute sprays is concerned, limited direct calculations or measurements are available. Tal *et al.* [16] have, however, calculated the heat and momentum transfer rates at a Reynolds number of 100 for dense sphere assemblages arranged in tandem. Interaction was shown by the results that the Nusselt number significantly decreased as droplet spacing decreases. Recently, Bellan and Harstad [17, 18] analyzed the convective evaporation for non-dilute droplet clusters. They suggested that for dense clusters the initial relative velocity between the gases and droplets is a weak parameter and the evaporation is diffusion-controlled in the cluster core. This result indicates that the simplified droplet-in-bubble approach may still be useful for the evaporation of non-dilute sprays even in convective flows. Experimental studies are required for a clearer understanding of convective evaporation within non-dilute sprays.

This paper presents the first part of a series of experimental studies of which the ultimate goal is to reveal the evaporation characteristics within non-dilute droplet clouds with the effects of convection and polydispersity included. Before the experiments for convective evaporation are conducted, baseline data of quiescent or weakly convective evaporation have to be obtained. Also, the reliability of the experimental method, which will be modified to extend to convective evaporation, may be carefully examined using quiescent or weakly convective, monodisperse clouds. In addition, these data of quiescent or weakly convective evaporation are needed for the evaluation of relevant evaporation theories.

The main objective of this first-stage work is to experimentally study the evaporation rate data for non-dilute and dilute monodisperse clouds under weakly convective conditions. In addition, an improvement of current droplet-in-bubble models will be made to simulate the experiments. The effects of convection and polydispersity are being investigated and will be presented in the future.

2. EXPERIMENTAL METHODS

Spray evaporation was conducted in a well insulated evaporation tube under weakly convective flow conditions at atmospheric pressure. The experimental apparatus, schematically shown in Fig. 1, consisted of three parts: (1) a monodisperse spray generator, (2) an evaporation tube, and (3) a Phase Doppler Particle Analyzer (PDPA). Nearly monosize sprays with negligible pre-existing fuel vapor were generated using

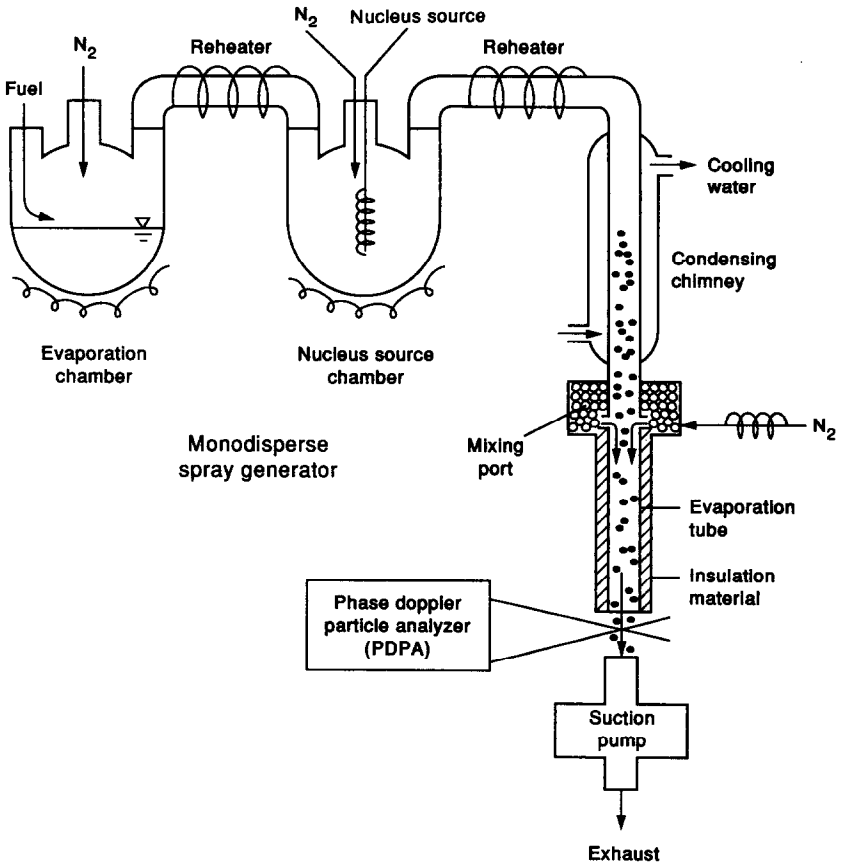

FIG. 1. Schematic of experimental apparatus.

the spray generator. The spray, carried by a nitrogen gas flow, was immediately led through the evaporation tube, which was initially at an elevated temperature. (In fact, it took approximately an hour to reach steady-state evaporation before actual measurements could be made.) At the center of the tube exit, spray parameters (including droplet diameter, droplet number density, droplet velocity, and gas velocity) were simultaneously measured using the PDPA. By varying the tube length, droplet diameters were obtained at various evaporation stages. Initial spray parameters were measured at the exit of the spray generator. The evaporation rate with respect to time could then be determined by knowing the droplet diameter variation and droplet velocity. The details of the experimental apparatus are described in the following section.

2.1. *Experimental apparatus*

Monodisperse spray generator. The design of the monodisperse spray generator was modified from the one used by Burgoyne and Cohen [19]. As shown in Fig. 1, it consisted of an evaporation chamber, a nucleus source chamber, reheaters, a condensing chimney, and a dilution port. The temperatures of the chambers and reheaters were controlled using temperature controllers. Nitrogen gas was first passed through the evaporation chamber where it was mixed with the fuel vapor. The nitrogen–fuel vapor mixture was then passed over the condensation nucleus source, which was an electrically heated nichrome coil coated with sodium chloride. Additional dispersion nitrogen was introduced into the nucleus source chamber for more uniform mixing. Having passed through a reheater, the mixture of fuel vapor, nitrogen and salt nuclei flowed through the condensing chimney, in which the fuel vapor cooled and condensed on the nuclei to form a nearly monosize spray. Since the vapor phase of the spray was saturated at this time, hot dilution nitrogen (78–85°C, depending on flow conditions) was introduced from the dilution port so that the fuel vapor concentration became far lower than the saturation value at the resultant mixture temperature (75°C). The dilution port was found to rapidly yield satisfactorily uniform gas temperature, flow velocity and droplet distribution after the first 5 cm of the evaporation tube (cf. Fig. 3 for droplet velocity, gas velocity, and number density distributions). The monodisperse sprays generated had size dispersities

of approximately 0.18,† mean diameters of 7 to 60 μm, and a wide droplet number density range (e.g. 50 to 5000 particles cm^{-3}).

Evaporation tube. The vaporless monodisperse spray generated immediately flowed through the insulated evaporation tube to undergo globally adiabatic evaporation. The evaporation tube was a 2 cm I.D. acrylic tube covered with insulation material, which was used to simulate an adiabatic evaporation environment and to avoid fuel condensation on the tube wall. Various tube lengths (2 to 65 cm) were used for the measurement of spray parameters at different evaporation stages. All the tubes were preheated to 75°C in a constant-temperature oven prior to experiment. Upward backflow due to buoyancy was eliminated using a suction pump at the tube exit.

Phase Doppler Particle Analyzer (PDPA). PDPA (one-component, Aerometrics) was used for simultaneous measurements of droplet diameter, droplet number density, droplet velocity, and gas velocity. The gas velocity was taken as the velocity of the very fine droplets (as small as 1 μm) existing in the spray. The PDPA is commercially available and is described by Bachalo and Houser [20]. The instrument was operated in 150° backward scatter geometry.

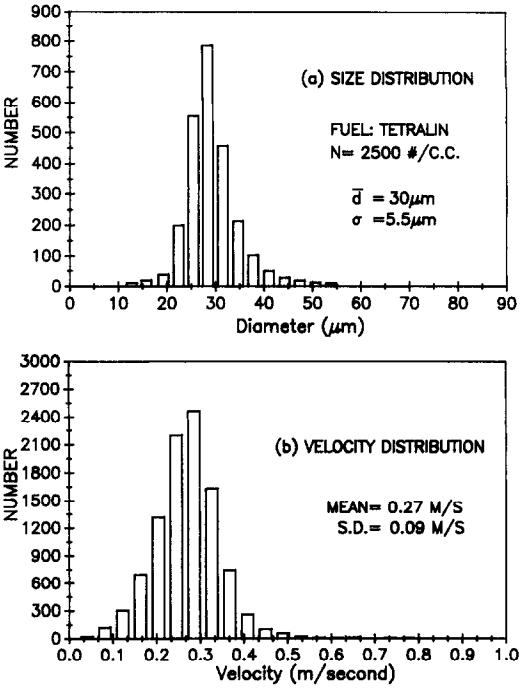

FIG. 2. Droplet diameter and velocity distribution of a monodisperse spray.

2.2. *Instrumentation*

Gas temperatures were measured using a chromel–alumel thermocouple having a 150 μm bead diameter. The temperature of the hot dilution nitrogen was controlled using a temperature controller. Nitrogen flow rates were determined using rotameters. The pre-existing fuel vapor concentration, approximately 1/20 to 1/60 of the saturation value at 75°C, was estimated based on the dilution nitrogen flow rate and the saturation concentration corresponding to the mixture temperature (38°C) at the exit of the spray generator.

Test samples for PDPA measurements were 10 000 for dense sprays and more than 5000 for dilute sprays.

2.3. *Experimental conditions*

Evaporation tests were conducted for tetralin (tetrahydronaphthalin, $C_{10}H_{12}$) sprays at atmospheric pressure. The initial gas and tube temperatures were 75°C, and the initial droplet temperature was taken as 38°C (i.e. the mixture temperature at the spray generator exit). Initial droplet diameters were fixed at 30 ± 1 μm (the peak value of the size distribution). (The peak value is called the mean diameter in this paper since it nearly equals the arithmetic mean diameter.) A representative initial size distribution is presented in Fig. 2.

The insulation of the evaporation tube was also examined. With the tube initially at 75°C, a 75°C nitrogen flow was passed through it. The temperature drop at the tube exit was no more than 3°C for a tube as long as 45 cm.

Flow conditions had been carefully examined prior to the experiments. This examination was conducted at typical test conditions except that flow temperatures were chosen at room temperature for simplicity. The radial distribution of droplet velocity, gas velocity, and droplet number density at two axial positions are shown in Fig. 3. The radial velocity distributions are rather uniform near the core region; the number density distributions are uniform except near the wall. The evaporation process along the centerline may, therefore, be considered to be one-dimensional. As shown in Fig. 3 for the two different axial positions (5 and 35 cm), the axial velocities change little after 5 cm. For all the experiments, the initial droplet Reynolds numbers (Re_d) were of the order of 0.01 for all experiments.

The experimental uncertainty for droplet volume fraction was 5%. The thermocouple yielded a ± 1°C uncertainty in gas temperature. It should be mentioned that the gas temperatures measured may be lower than the actual ones due to the effect of droplet collisions on the thermocouple. Uncertainties for droplet diameter, droplet velocity and droplet number density, according to manufacturer specifications, were ± 1 μm, 2% and 10%, respectively. Mean droplet diameters were also examined using the Fraunhofer diffraction method [21] and the impactor method [22] with an impactor coefficient of 0.86 [23]. Careful examinations indicated a mean diameter uncertainty of 2 μm.

† Size dispersity is defined as $\sigma/\bar{d}$, where $\bar{d}$ is the mean droplet diameter and σ is the standard deviation of the diameter distribution. In general, a spray having a size dispersity less than 0.2 can be considered as monodisperse.

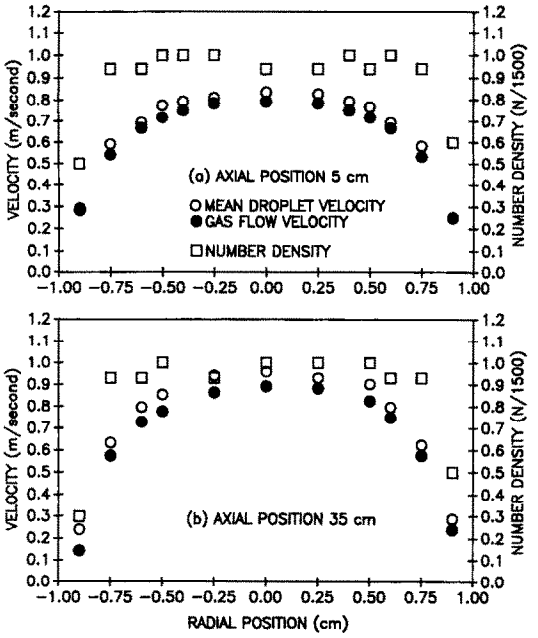

FIG. 3. Radial distributions of droplet number density, droplet velocity, and gas velocity at various axial positions.

3. THEORETICAL WORK

The droplet-in-bubble approach, which is suitable for quiescent or weakly convective conditions, was used to simulate the experiments. In addition to the three existing models [11–13], a fourth version was adopted in the present study. This version essentially follows the model of Bellan and Cuffel [13]. A differential formulation was, however, used, as in Tishkoff's model, instead of the integral form to relax the unity-Lewis-number limitation in Bellan and Cuffel's model. Another difference is that simple cubic instead of the face-centered cubic droplet arrangement [13] is used presently.

As in ref. [13], each droplet has a sphere of influence (bubble region), the radius of which is the half-distance between the centers of the neighboring droplets, with an edge volume associated with it. The differential equations of mean species and energy conservation in the bubble region are identical to Tishkoff's [12]. Equations for mass and energy balance in the lumped edge region are

$$\rho_e V_e \frac{dY_e}{dt} = -4\pi \cdot r_s^2 \cdot D_s \frac{\partial Y}{\partial r}\bigg|_s + \frac{\partial}{\partial t}\left(\int_{r_s}^{r_e} \rho Y 4\pi r^2 \, dr\right) \quad (1)$$

and

$$\rho_e C_{pe} V_e \frac{dT_e}{dt} = -4\pi \cdot r_s^2 \cdot k_s \frac{\partial T}{\partial r}\bigg|_s + \frac{\partial}{\partial t}\left(\int_{r_s}^{r_e} \rho C_p T 4\pi r^2 \, dr\right). \quad (2)$$

Table 1. The properties of the tetralin–nitrogen mixture used in computation†

$C_p = 0.331$	cal $g^{-1}\,°C^{-1}$
$k = 6.40 \times 10^{-5}$	cal $cm^{-1}\,s^{-1}\,°C^{-1}$
$\rho = 1.01 \times 10^{-3}$	g $cm^{-1}\,s^{-1}$
$\mu = 1.85 \times 10^{-4}$	g $cm^{-1}\,s^{-1}$
$\alpha = 0.192$	$cm^2\,s^{-1}$
D‡ $= 0.083$	$cm^2\,s^{-1}$
$L = 72$	cal g^{-1}

† The values presently listed, except L, were estimated using the 1/3-rule [24] based on the initial edge temperature (75°C) and the initial droplet temperature (38°C). These values were, however, time-varied based on the edge temperature and the droplet temperature in actual calculations. The determination of tetralin vapor properties followed Chan and Wu [23].

‡ Mass diffusivity was calculated using the Chapman and Enskog formula [25].

Boundary conditions for mass and energy balance at the droplet surface follow Tishkoff [12].

The properties of tetralin used in computation are listed in Table 1.

4. RESULTS AND DISCUSSION

To study droplet interaction on evaporation, a series of tests were performed with respect to droplet spacing, with evaporation rates and evaporation times (saturation times or complete evaporation times) determined. Corresponding theoretical simulations based on the present version of droplet-in-bubble model as well as some other droplet-in-bubble models, were also made and compared with the experimental data. It should be mentioned that complete insulation was difficult to obtain, although the evaporation tube was carefully insulated during the experiments. Considering this, temperature drops due to the heat loss from the tube wall have been accounted for in model calculations, as shown in Appendix A.

Figure 4 shows the experimental evaporation-rate data together with the calculations of different models for a nondilute as well as a dilute spray. The plots are expressed in terms of remaining droplet volume fractions vs time, with each data point representing an average of three runs with an uncertainty of 5%.

For the more dilute case ($N = 210$ droplets cm^{-3}, $s/d_0 = 56$) shown in Fig. 4(a), droplet interaction was rather weak, and the droplets evaporated to completion in a manner resembling single droplets. For this case, all the four theories exhibit good performance. For the non-dilute case ($N = 2100$ droplets cm^{-3}, $s/d_0 = 26$) shown in Fig. 4(b), the evaporation rate was greatly reduced due to strong droplet interaction. Evaporation ceased due to saturation at approximately 0.5 s. As far as the theories are concerned, the present model is still in excellent agreement with the experimental data for both the saturation time and droplet volume fraction history. The model of Bellan and Cuffel [13] also appears satisfactory, but the models of Zung [11] and Tishkoff

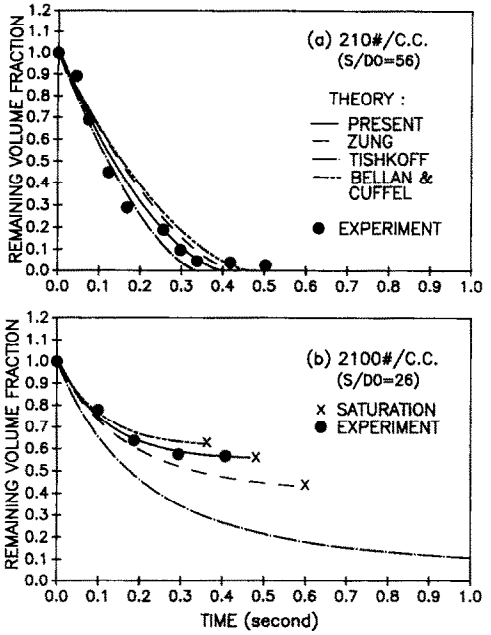

FIG. 4. Comparison of theoretical calculations of remaining volume fraction vs time with experimental data.

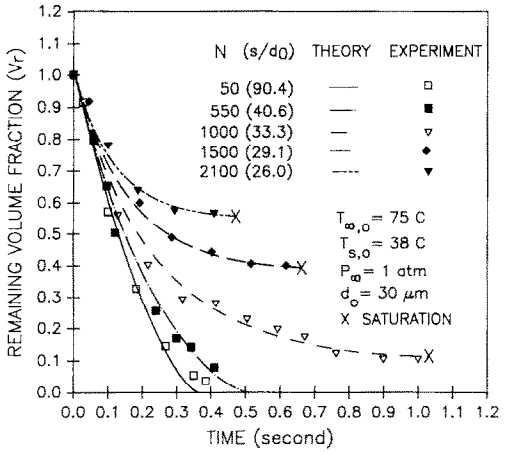

FIG. 5. Remaining droplet volume fractions vs time for various droplet number densities.

[12] exhibit significant deviations for this non-dilute spray.

The deviation of Zung's model is due to its crudity as described previously. Tishkoff's model is inaccurate because it imposes less rigorous boundary conditions at the bubble surface. The major improvement of the present model over that of Bellan and Cuffel is the relaxation of the $Le = 1$ assumption.

Figure 5 compared the evaporation rate data obtained from the present theory and experiment for a range of droplet number densities (50 to 2100 droplets cm^{-3}). As $N = 50$ ($s/d_0 = 90.4$), droplet interaction was insignificant in this very dilute spray, with droplets evaporating to completion in a manner resembling single droplets. As $N = 550$ ($s/d_0 = 40.6$), weak interaction slightly reduced the evaporation rate to cause a slightly longer time for complete evaporation. As $N = 1000$ ($s/d_0 = 33.3$), the evaporation rate was further decreased because of the accumulation of fuel vapor and the cooling of the surrounding gas (cf. Fig. 6 for gas temperature variations). Evaporation was found to cease at approximately 1.0 s in this case due to fuel vapor saturation. As N is further increased ($N = 1500$ or 2100), evaporation was further retarded to yield earlier saturation. As far as theoretical calculations are concerned, excellent agreement between the theory and experiment is clearly shown for both evaporation rates and evaporation times in all cases. The present model appears, therefore, to accurately account for the interaction between droplets for arbitrary droplet spacings. The monotonic decrease of evaporation rate with decreasing droplet spacing, as shown in Fig. 5, was not correctly predicted by Tishkoff [12]. His model indicated that the evaporation rate would exceed that of a single droplet at a moderately large s/d_0 (10 to 100 in his examples). Tishkoff's physically unreasonable result presumably resulted from the crude treatment of boundary conditions at the bubble surface.

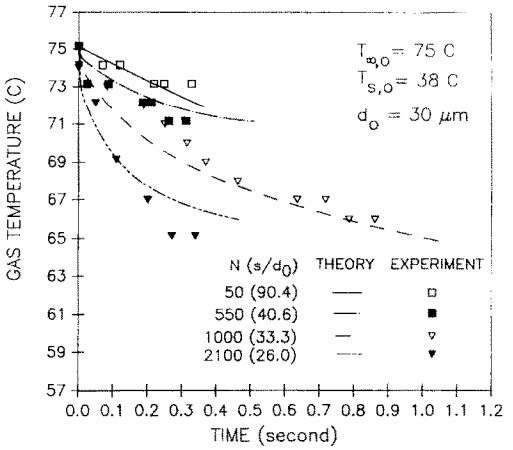

FIG. 6. Gas temperatures vs time for various droplet number densities.

The gas temperature histories corresponding to the above cases are shown in Fig. 6. Corrections have been made for the heat loss from the tube wall, as in Appendix A. The theory and experiment again agree satisfactorily. Figure 6 indicates that ambient gas temperatures decrease monotonically during the evaporation processes, with larger decreases for denser sprays. The cooling of ambient gas resulted from the energy consumption in droplet heating and phase transition. Since the evaporation rate is rather sensitive to ambient temperature, the cooling of ambient gas should be another important reason for evaporation retardation besides vapor accumulation.

Figure 7 shows the experimental and theoretical results of the times for complete evaporation or saturation as well as the remaining droplet volume frac-

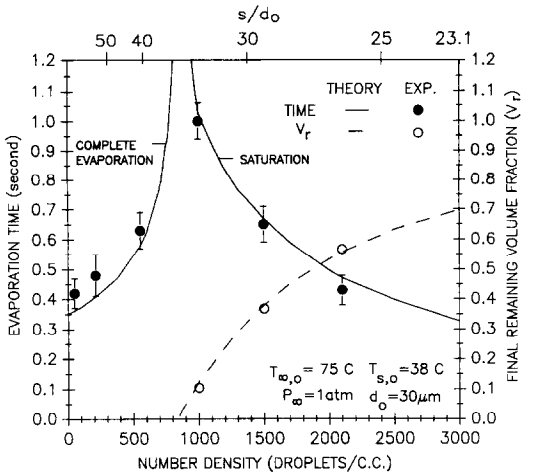

FIG. 7. Evaporation times and final remaining volume fractions vs droplet number density.

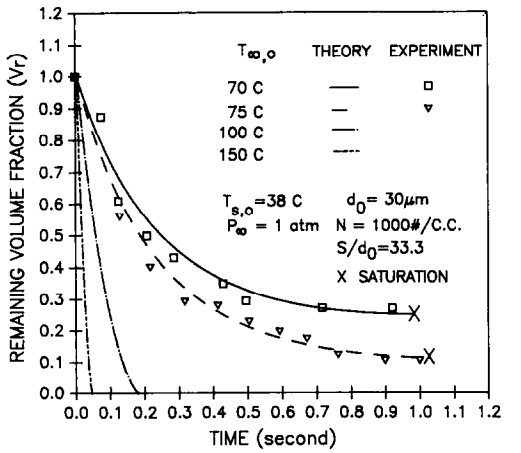

FIG. 8. Remaining droplet volume fractions vs time for various initial gas temperatures.

tions at saturation with respect to N. In Fig. 7, there are two different regions with the transition occurring at approximately $N = 800$. For $N < 800$, droplets evaporate completely before saturation. As N is gradually increased, strong droplet interaction appears and, as $N > 800$, saturation occurs before complete evaporation. For a larger N, saturation occurs earlier, leaving more liquid fuel unvaporized. Large uncertainties of experimental saturation times might exist because it was difficult to judge the exact saturation times when evaporation ceased, since droplet volume fraction changed very slightly near saturation.

In Fig. 8, evaporation rate histories at various ambient gas temperatures were compared for $N = 1000$ droplets cm^{-3} ($s/d_0 = 33.3$). The excellent accuracy in both cases justifies high reliability of the theoretical predictions at high temperatures, although experiments were only conducted at low temperatures (70 and 75°C). Figure 8 indicates that the evaporation rate depends strongly on gas temperature and a slight temperature increase would greatly reduce the evaporation time. In addition, while saturation occurs at 75°C, complete evaporation is reached at a slightly higher temperature of 100°C. In other words, while at a fixed s/d_0 a cloud at a low temperature is non-dilute in the sense that evaporation interaction is strongly manifested, it may be dilute at a higher temperature. As far as evaporation is concerned, therefore, the value of s/d_0 as an indicator of whether a spray or cloud is dilute or non-dilute is temperature dependent. The smaller evaporation time (or the larger evaporation rate) at a higher temperature can be attributed to the combination of a higher heat transfer rate (due to both a larger temperature difference and a larger α), a larger D, and a larger saturation vapor pressure (cf. Fig. B1).

5. SUMMARY AND CONCLUSIONS

A quantitative experimental study on the droplet evaporation in non-dilute as well as dilute monodisperse sprays was performed at atmospheric pressure. Evaporation was carried out in an insulated evaporation tube under weakly convective flow conditions. The sprays used for the experiment were nearly monosize. With mean droplet diameters, droplet number densities, droplet velocities, and gas velocities measured optically using a PDPA at various stages, the evaporation rate histories were determined. Gas temperature histories were measured using a thermocouple. An improved version of the droplet-in-bubble evaporation model for non-dilute monodisperse sprays was proposed. To examine the reliability of predictions, the present model, as well as others [11–13], was applied to simulate the experiments. Both the evaporation rate and gas temperature histories were shown to be accurately predicted by the present model. The model of Bellan and Cuffel [13] was also satisfactory.

Both experiments and calculations indicated that droplet interaction increased with increasing N (or decreasing s/d_0). At a small N, droplets evaporated to completion as single droplets. As N was increased, the evaporation time increased monotonically and eventually saturation would occur before complete evaporation when N was beyond a transitional value.

Our future work will include convection and polydispersity effects.

Acknowledgements—The authors are grateful to Dr K.-K. Chan for the initial development of the monodisperse spray generator. The assistance and discussion offered by Dr D.-M. Chen and Dr S.-D. Jang throughout this study are also acknowledged.

REFERENCES

1. G. M. Faeth, Evaporation and combustion of sprays, *Prog. Energy Combust. Sci.* **9**, 1–76 (1983).
2. N. A. Chigier and C. G. McGreath, Combustion of droplets in sprays, *Acta Astronautics* **1**, 687–710 (1974).

3. H. H. Chiu and T. M. Liu, Group combustion of liquid droplets, *Combust. Flame* **17**, 127–142 (1977).
4. C. K. Westbrook, Numerical solution of the spray equation, Lawrence Livermore Laboratory UCID-17361 (1976).
5. T. A. Brzustowski, E. M. Twardus, S. Wojcicki and A. Sobiesiak, Interaction of two burning droplets of arbitrary size, *AIAA J.* **17**, 1234–1242 (1979).
6. K. Miyasaka and C. K. Law, Combustion of strongly-interacting linear droplet arrays, *18th Symp. (Int.) on Comb.*, pp. 283–292 (1981).
7. A. S. M. Nuruzzaman, A. B. Hedley and J. M. Beer, Combustion rates in self-supporting flames on monosized droplet streams, *J. Inst. Fuel* **43**, 301–310 (1970).
8. J. J. Sangiovanni and M. Labowsky, Burning times of linear fuel droplet arrays: a comparison of experiment and theory, *Combust. Flame* **47**, 15–20 (1982).
9. A. Umemura, S. Ogawa and N. Oshima, Analysis of the interaction between two burning fuel droplets with different sizes, *Combust. Flame* **43**, 111–119 (1981).
10. M. Labowsky, Calculation of the burning rates of interacting fuel droplets, *Combust. Sci. Technol.* **22**, 217–226 (1980).
11. J. T. Zung, Evaporation rate and lifetimes of clouds and sprays in air—the cellular model, *J. Chem. Phys.* **46**, 2064–2070 (1967).
12. J. M. Tishkoff, A model for the effect of droplet interaction on vaporization, *Int. J. Heat Mass Transfer* **22**, 1407–1415 (1979).
13. J. Bellan and R. Cuffel, A theory of nondilute spray evaporation based upon multiple drop interactions, *Combust. Flame* **25**, 55–67 (1983).
14. C. K. Law, Adiabatic spray vaporization with droplet temperature transient, *Combust. Sci. Technol.* **15**, 65–74 (1977).
15. S. D. Jang and H. H. Chiu, Theory of renormalized droplet: II. Non-steady vaporization of droplet in nondilute sprays, AIAA paper No. 88-0639, Reno, Nevada (1988).
16. R. Tal, D. N. Lee and W. A. Sirignano, Hydrodynamics and heat transfer in sphere assemblages—cylindrical cell models, *Int. J. Heat Mass Transfer* **26**, 1265–1273 (1983).
17. J. Bellan and K. Harstad, Analysis of the convective evaporation of nondilute clusters of drops, *Int. J. Heat Mass Transfer* **30**, 125–136 (1987).
18. J. Bellan and K. Harstad, The details of the convective evaporation of dense and dilute clusters of drops, *Int. J. Heat Mass Transfer* **30**, 1083–1093 (1987).
19. J. H. Burgoyne and L. Cohen, The effect of drop size on flame propagation in liquid aerosols, *Proc. R. Soc. London A* **225**, 375–392 (1954).
20. W. D. Bachelo and M. J. Houser, Development of the phase/doppler spray analyzer for liquid drop size velocity characterizations, AIAA paper No. 84-1199, Cincinnati, Ohio (1984).
21. J. Cornillault, Particle size analyzer, *Appl. Optics* **22**, 265–268 (1972).
22. K. R. May, The measurement of airborne droplets by the magnesium oxide method, *J. Sci. Instrum.* **27**, 128–130 (1950).
23. K. K. Chan and T. M. Wu, An experimental and theoretical investigation of the transition phenomenon in fuel spray deflagration 2. The model, *Fuel* **68**, 139–144 (1989).
24. G. L. Hubbard, V. E. Denny and A. F. Mills, Droplet evaporation: effects of transients and variable properties, *Int. J. Heat Mass Transfer* **18**, 1003–1008 (1975).
25. A. M. Kanury, *Introduction to Combustion Phenomena*, pp. 48–55. Gordon and Breach, New York (1975).
26. N. B. Vargaftik, *Handbook of Physical Properties of Liquids and Gases*, 2nd Edn, pp. 433–476. Hemisphere, New York (1976).

APPENDIX A: CORRECTION OF TEMPERATURE DROPS DUE TO HEAT LOSS FROM TUBE WALL

The temperature drops due to the heat loss from the tube wall were experimentally determined. With the tube initially at 75°C, a 75°C nitrogen flow was passed through it. The temperature drops were then measured along the tube center.

Measurements indicated that the temperature drop was approximately linear with the axial distance and that the drop at 45 cm was 3°C, independent of flow velocity. Accordingly, the following correction was made to the raw model calculations:

$$\Delta T = \int \left(\frac{3}{45}\right) \cdot v_g \cdot \mathrm{d}t \quad ^\circ\mathrm{C\,cm^{-1}}.$$

APPENDIX B: THERMAL DIFFUSIVITIES (α), MASS DIFFUSIVITIES (D), AND EQUILIBRIUM DROPLET SURFACE TEMPERATURES FOR THE TETRALIN–NITROGEN MIXTURE

In our evaporation model, the transport properties (α, D, μ, etc.) are spatially uniform but time-varying. They were determined using the 1/3-rule [24] based on the droplet surface temperature and bubble boundary temperature.

The calculation of D of the tetralin–nitrogen mixture followed the Chapman–Enskog formula [25]. The determination of α was based on

$$\alpha = k/(\rho \cdot C_p)$$

where k, ρ, and C_p are the thermal conductivity, density, and constant pressure heat capacity of the tetralin–nitrogen mixture.

The determination of the properties of tetralin vapor followed Chan and Wu [23] and those of nitrogen followed Vargaftik [26].

Representative values of α, D and T_s are shown in Fig. B1 with respect to T_{∞}.

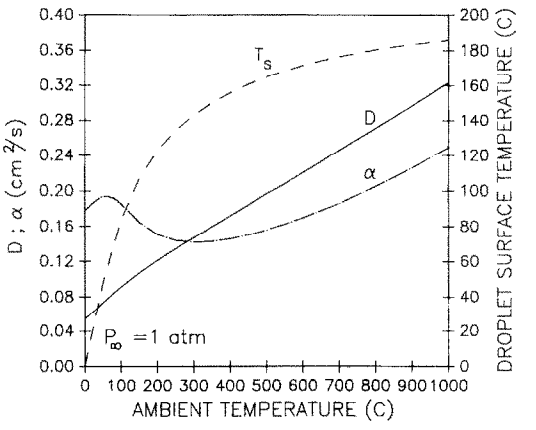

FIG. B1. Thermal diffusivities (α), mass diffusivities (D), and equilibrium droplet surface temperature (T_s) vs ambient gas temperature for the tetralin–nitrogen mixture.

EVAPORATION DES GOUTTELETTES MONODISPERSEES DANS DES NUAGES DILUES OU NON

Résumé—On étudie expérimentalement et théoriquement l'évaporation de gouttelettes dans des nuages dilués ou non de gouttelettes monodispersées. Cette étude présente des données quantitatives expérimentales, dans le cas d'un tube évaporatoire isolé et de conditions d'écoulement à la pression atmosphérique avec vitesse faible. On utilise des nuages de tétraline dont les gouttes ont presque la même taille autour de 30 μm de diamètre. Pour un nuage non dilué, l'évaporation est significativement plus faible que pour une goutte unique et l'évaporation peut s'arrêter à cause de la saturation. Une version améliorée du modèle adopté pour décrire l'évaporation dans des nuages monodispersés non dilués, montre une excellente simulation des expériences.

VERDAMPFUNG VON UNVERDÜNNTEN UND VERDÜNNTEN MONODISPERSEN TROPFENWOLKEN

Zusammenfassung—Die Verdampfung von Tropfen in unverdünnten und verdünnten monodispersen Tropfenwolken wird experimentell und theoretisch untersucht. In der vorliegenden Arbeit werden quantitative Versuchsdaten für die monodisperse Wolkenverdampfung vorgestellt. Die Versuche werden in einem isolierten Verdampfungsrohr bei schwachen Konvektionsströmungen unter Atmosphärendruck durchgeführt. Dabei werden Tetralinwolken mit nahezu einheitlicher Tropfengröße (mittlerer Durchmesser 30 μm) verwendet. Für die untersuchte nichtverdünnte Wolke kann festgehalten werden, daß die Verdampfungsgeschwindigkeit wesentlich kleiner ist als bei einem Einzeltropfen und daß die Verdampfung aufgrund eintretender Sättigung zum Stillstand kommen kann. Zur Beschreibung der Verdampfung in nichtverdünnten monodispersen Wolken wird eine verbesserte Version des Modells eines Tropfens in einer Blase herangezogen, wodurch sich die Versuchsergebnisse hervorragend simulieren lassen.

ИСПАРЕНИЕ НЕРАЗРЕЖЕННЫХ И РАЗРЕЖЕННЫХ ОБЛАКОВ МОНОДИСПЕРСНЫХ КАПЕЛЬ

Аннотация—Экспериментально и теоретически исследуется испарение капель в неразреженных и разреженных облаках монодисперсных капель. Приводятся экспериментальные данные для испарения монодисперсных облаков. Эксперименты проводятся в изолированной испарительной трубе в условиях слабоконвективного течения при атмосферном давлении. Используются близкие к монодисперсным облака тетралина со средним диаметром капель, составляющим 30 мкм. Скорость испарения неразреженного облака существенно ниже, чем для одной капли, и испарение может прекратиться благодаря насыщению. Усовершенствованный вариант модели капли в пузырьке, используемый для описания испарения в неразреженных монодисперсных облаках, хорошо описывает эксперименты.